Low replication stress leads to specific replication timing advances associated to chromatin remodelling in cancer cells.

Lilas Courtot[1], Chrystelle Maric[2], Elodie Bournique[1], Laure Guitton-Sert[1], Miguel Madrid-Mencia[1], Vera Pancaldi[1], Jean-Sébastien Hoffmann[1,3], Jean-Charles Cadoret[2*], Valérie Bergoglio[1*].

[1]Centre de Recherches en Cancérologie de Toulouse (CRCT), UMR1037 Inserm, ERL5294 CNRS, 2 Avenue Hubert Curien, 31037, Toulouse, France. University Paul Sabatier III, Toulouse, France.
[2] Pathologies de la Réplication de l'ADN, Université de Paris, Institut Jacques Monod, UMR7592, CNRS, F-75006, Paris, France.
[3]Laboratoire de pathologie, Laboratoire d'excellence Toulouse Cancer, Institut Universitaire du Cancer-Toulouse, Oncopole, 1 avenue Irène-Joliot-Curie, 31059 Toulouse cedex, France
**co-last authors*.

V.B., corresponding author: valerie.bergoglio@inserm.fr

Abstract

DNA replication is very well orchestrated in mammalian cells due to a tight regulation of the temporal order of replication origin activation, known as the replication timing program. The replication timing of a given replication domain is very robust and well conserved in each cell type. Upon low replication stress, the slowing of replication forks induces delayed replication of some fragile regions leading to DNA damage and genetic instability. Except for these fragile regions, the direct impact of low replication stress on the replication timing in different cellular backgrounds has not been explored in detail.

Here we analysed DNA replication timing across the whole genome in a panel of human cell lines in the presence of low replication stress. We demonstrate that low replication stress induced by aphidicolin has a stronger impact on the replication timing of cancer cells than non-tumour cells. Strikingly, we unveiled an enrichment of specific replication domains undergoing a switch from late to early replication in some cancer cells. We found that advances in replication timing correlate with heterochromatin regions poorly sensitive to DNA damage signalling while being subject to an increase of chromatin accessibility in response to aphidicolin. Finally, our data indicate that, following release from replication stress conditions, replication timing advances can be inherited by the next cellular generation, suggesting a new mechanism by which some cancer cells would adapt to cellular or environmental stress.

Background

DNA replication is a highly complex process that ensures the accurate duplication of the genome, ensuring the faithful transmission of genetic material to the cell's progeny. DNA replication is operational during S phase through the replisome activity, but it requires important upstream regulation during the G1 phase and checkpoints in G2 phase, together with a tight control all along the process itself. Multicomplex replication machinery performs the coordinated initiation of DNA synthesis at hundreds of replication origins spread throughout the whole length of the genome (Masai et al., 2010). Adjacent origins that initiate DNA replication at the same moment have been called "replicon clusters" (Berezney et al., 2000), giving rise to synchronously replicating chromosomal domains. Each replicon cluster starts replicating at a precise moment during the S-phase, either in the beginning (Early-S), the middle (Mid-S) or the end (Late-S). This coordination of the temporal program of DNA replication is called "replication timing" (RT), allowing a complete and faithful duplication of the entire genome before cell division.

The RT program is modified during organism development and cellular differentiation (Hiratani et al., 2008; Pope et al., 2010) and is coupled with gene expression, chromatin epigenome and nuclear 3D compartmentalization (Hiratani et al., 2010; Julienne et al., 2015; Madrid-Mencía et al., 2020; Rivera-Mulia et al., 2015). In somatic cells, the RT pattern is very robust through cell generations (Rivera-Mulia et al., 2015; Ryba et al., 2010, 2011; Takahashi et al., 2019) with early-replicating DNA residing in the interior of the nucleus while the later-replicating regions are present at the nuclear periphery or near the nucleolus (Goren and Cedar, 2003; Jackson and Pombo, 1998; Ryba et al., 2010) in correspondence with the A and B compartments, containing active and inactive chromatin, respectively. Additional complex associations have been highlighted such as the link between early-replicating regions and GC nucleotides enrichment, enhanced gene expression, and active epigenetic marks corresponding to open or euchromatin. On the other hand, late-replicating regions tend to be enriched in AT nucleotides, low gene content, and have heterochromatin repressive epigenetic marks (Donley and Thayer, 2013; Goren and Cedar, 2003).

DNA replication stress is defined as the slowdown or stalling of the replication fork resulting in inefficient DNA replication. Many exogenous or endogenous sources of impediment on DNA as well as pathological perturbations such as oncogene activation,

conflicts between DNA replication and transcription or shortage of nucleotides affect the progression of replication forks, inducing replication stress (Gómez-González and Aguilera, 2019; Jones et al., 2013; Kotsantis et al., 2018; Magdalou et al., 2014; Miron et al., 2015). Experimentally, replication stress can be induced by the specific inhibition of replicative DNA polymerases by treatment with the drug aphidicolin. Notably, low doses of aphidicolin (0.1 to 0.5µM) are well known to cause the induction of common fragile site (CFS) expression and the generation of under-replicated DNA that leads to DNA damage transmission (Chan et al., 2009; Harrigan et al., 2011; Hecht and Glover, 1984; Lukas et al., 2011; Naim and Rosselli, 2009). CFSs are chromosomal regions harbouring some cancer-related genes (Ozeri-Galai et al., 2012) that are prone to breakage upon replication stress (Arlt et al., 2003) and whose instability is often observed at the early stages of carcinogenesis (Gorgoulis et al., 2005). The fragility of these chromosomal regions has been widely studied, revealing that incomplete DNA replication before mitosis (Harrigan et al., 2011; Ji et al., 2020; Lukas et al., 2011; Macheret et al., 2020) mainly due to conflicts with large transcription units (Brison et al., 2019; Le Tallec et al., 2013; Sarni et al., 2020) or origin paucity (Letessier et al., 2011; Wilson et al., 2015) are major causes.

Evidence of aberrant RT in many different genetic diseases and cancers suggest the importance of this cellular process for genomic stability (Rivera-Mulia et al., 2017, 2019; Ryba et al., 2012). Interestingly, replication stress inducing CFSs expression also affects the RT of these specific chromosomal domains (Brison et al., 2019; Sarni et al., 2020). The extent to which these RT changes influence the normal or tumour transformation process is still largely unknown.

One aim of the study was to question if differential response to low replication stress could be due to diverse cellular backgrounds or to a common mechanism, independent of cell type and origin. To do so, we characterized and compared the consequences of mild replication stress induced by low doses of aphidicolin on 4 cancer and 2 non-tumour human cell lines (colon, blood, osteoblast, retina, and lung) (**Table S1**). Our experiments revealed that low doses of aphidicolin have a stronger impact on the RT of cancer cells, promoting some RT delays but also some unexpected RT advances. We demonstrated that RT advances loci can be housed in CFS but contrary RT delays, they are poorly targeted by DNA damage signalling but characterized by stronger chromatin accessibility in response to aphidicolin. Finally, we observed the persistence of RT advances in daughter cells released from replication stress which is correlated with modification of chromatin loop size and pre-RC loading in G1 and an

increase in the expression of genes contained in these chromosomic regions. Altogether, our results indicate that low replication stress which lead to RT advances onto flexible heterochromatin regions influence the DNA replication program and gene expression of the next generation of cancer cells.

Results

Low replication stress differentially impacts cancer and non-tumour cells

In order to evaluate cellular responses to mild replication stress, we treated cells with 0.2µM aphidicolin and used DMSO as a control. We used 6 well characterized cell lines that are common models (HCT116, RKO, U2OS, K562, MRC5-N and RPE-1) and that differ according to tissue origin, tumorigenicity, differentiation stage and molecular characteristics such as oncogene expression, genetic instability type and telomere maintenance mechanisms (**Table S1**). The duration of aphidicolin treatment was adapted to each cell line in order to treat a maximum number of cells in S phase for a single generation. We selected the longest treatment duration that maintained a minimum of BrdU positive cells in G1 phase ensuring that no cells were treated during two consecutive cell cycles (**Table S2** and **Fig S1a**). This optimal treatment duration was also determined in order to analyse the consequences of replication stress in the daughter cells released from the drug.

Analysis of the S phase checkpoint induction at the end of aphidicolin treatment, by monitoring Chk1 phosphorylation on serine 345, revealed a low level of checkpoint activation compared to acute replication stress (HU, 2mM 4h), with nevertheless a tendency of higher p-Chk1 level in cancerous cells (**Fig S1 b, c**). We furthermore noticed a global accumulation of cells in the S andG2/M phase under aphidicolin treatment, which again was more pronounced in cancerous cells (**Fig S1d, e**).

To study the impact of low replication stress exposure on the RT, we treated cells with aphidicolin 0.2µM for the appropriate time (**Table S2** and **Fig S1a**). At the end of the treatment, BrdU was added to the culture medium before cell sorting in two S-phase fractions (S1, S2) and global RT was analysed after hybridization of the neo-synthesized DNA on human whole genome microarrays, as previously described (Almeida et al., 2018; Fernandez-Vidal et al., 2014; Hadjadj et al., 2016) (**Fig S2a**). RT differential analyses were performed on biological replicate experiments using the START-R suite software (Hadjadj et al., 2020) and only significant modifications between aphidicolin and control condition were retained.

It has been reported that the RT profile of somatic cells is closely related to the cell type and tissue origin (Ryba et al., 2011). By performing a hierarchical clustering of RT for the different cell lines, we found that in absence of replication stress, non-tumour cells clustered together (cluster 1) and are separated from cancer cells (cluster 2) (**Fig 1a**). In the cluster 2, we observed that the replication timing of RKO is closer to HCT116, consistent with the fact that they are both colon cancer with microsatellite instability due to mismatch repair deficiency (MMR-) cell lines **(Table S1)**. The hierarchical clustering of RT after aphidicolin still maintains the two distinct cancer and non-tumour cells clusters but changes the distances within the cancer cells. Indeed, the RT of RKO cells appear to be closer to the K562 cells and HCT116 closer to U2OS (**Fig 1b**). Overall, this observation indicates first that without any replication stress, RT is sufficient to classify non-tumour and cancer cells, and second that aphidicolin treatment affects even more the cellular identity of cancer cells as we observed that RT of the two colon cancer cell lines (RKO and HCT116) are not anymore the closest within the cancer cells cluster 2 (**Fig 1b**).

Advance RT signature in cancer cells

We recapitulated the genome wide percentage of altered RT in the different cell lines in response to aphidicolin treatment (**Fig 1a**). Normal RPE-1 and MRC5-N cells were the least impacted cell lines with 1.54% and 1.94% of the genome undergoing RT alterations respectively (**Fig 1c**) while the RT in cancerous cells was globally more impacted by low replication stress. We noticed that the RKO cell line showed the highest response with 6.54% of the genome impacted (**Fig 1c,e** and large visualization of chromosomes in **Fig S3**).

Analysis of the aphidicolin-RT-impacted loci (aRTIL) led to the identification of regions with significant RT delays (DEL aRTIL), as previously reported (Brison et al., 2019; Sarni et al., 2020) (**Fig 1c,d**). In RPE-1 and HCT116, these DEL aRTIL represent the majority of impacted loci with 38/47 and 74/96 loci respectively. Importantly, in all cell lines, we also observed significant RT switches towards earlier RT (RT advances; ADV aRTIL) (**Fig 1c-e**). These ADV aRTIL represent the main type of RT changes in RKO cells, with the largest size (**Fig 2b** and **Fig S3**) and strongest amplitude (**Fig 1e** and **Fig S3**). To exclude the possibility that RT advances were experimental artefacts, we validated 3 ADV aRTIL by BrdU-ChiP-qPCR approach in the RKO cell line, confirming that the identified advanced domains are significantly replicated earlier (relative to BrdU incorporation) upon aphidicolin treatment. We also verify that

unmodified early and late RT domains were mostly replicated in their respective Early-S and Late-S fractions, without significant difference between the untreated and aphidicolin treated condition (**Fig S2b**).

To explore the potential similarities of RT modifications between cell lines, we quantified the number of common DEL and ADV aRTIL (**Fig 1f, g**). We found 9 common large ADV domains in RKO and K562 cells and 4 common ADV aRTIL in U2OS and MRC5-N. The few ADV domains detected in RPE-1 and HCT116 were mainly specific to each cell line. Both no-tumour cell lines (RPE-1 and MRC5-N) shared a majority of DEL aRTIL (14 common) and also have many in common with U2OS (8 and 6 with RPE-1 and MRC5-N respectively) and HCT116 cell lines (11 and 6 with RPE-1 and MRC5-N respectively). In contrast, DEL aRTIL found in RKO and K652 cells were poorly shared with other cell lines.

Collectively, these data demonstrate that RT is significantly modified in cancer cells for subset genomic domains in response to mild replication stress. RT of non-tumour cells RPE-1 and MRC5-N was less affected, in accordance with the lower induction of the S-phase checkpoint. Importantly, these data reveals for the first time that, in addition to delayed RT as shown in prior studies, RS can also induce RT advances. Finally, the overlapping of aRTIL between cell lines highlights two main distinct RT modification signatures: the first one in RKO and K562 cell lines, characterized by major shared RT advances in specific genomic domains and the second for U2OS, HCT116, MRC5-N and RPE-1 that are mainly enriched in the same RT delayed genomic regions.

ADV aRTIL are housed in heterochromatin late replicated chromosomic regions.

To explain the differential RT modifications between cell lines and chromosome loci, we first chose to explore histone modifications and other epigenomic features such as Laminar-Associates-Domains (LADs) and chromatin accessibility (DNase-seq) to identify a characteristic aRTIL epigenomic signatures. Given that the most advanced domains in RKO are shared in K562 we used public epigenomic data on K562 to characterize ADV aRTIL. First, this approach allowed us to validate our experimental RT by the observation of enrichment of the typical chromatin marks of Early, Mid and Late replicated regions (**Fig 2a,b** and **Fig S4**). For instance, Early replicated regions are enriched in euchromatin marks such as H3K27ac and H3K9ac while Late replicated regions correlate with heterochromatin marks (H3K9me3) and with LaminB1 (LADs) (**Fig 2a,b** and **Fig S4**). We also confirmed that chromatin accessibility

(DNAse-seq) decreases from Early to Late replicated regions. Interestingly, chromatin features of the ADV aRTIL are similar to those of late replicated domains and we noticed that they are even more enriched in H3K9me3 histone mark and in LaminB1, while they are poorer in the H3K27me3 mark, and display very low chromatin accessibility (**Fig 2a,b)**. This result suggests that ADV aRTIL domains belong to constitutive heterochromatin while DEL aRTIL are more like Mid-replicated regions (**Fig 2b**).

We next investigated if genomic features can help to distinguish ADV and DEL aRTIL. In accordance with the epigenomic features, we showed that in untreated cells, the large majority of ADV aRTIL were initially replicated in Late S-phase while DEL aRTIL were mainly replicated in the Early- Mid S-phase (**Fig S4a**). At the genomic sequence level, we observed that ADV aRTIL are large regions **(Fig 2c)** that share similar features with late replicating regions: poor GC content (**Fig 2d**), few constitutive origins (**Fig 2e**) and poor in genes (**Fig 2f**). In contrast, we found that DEL aRTIL are enriched for these features, especially in gene coverage (**Fig S4e**), and are thus closer to mid and/or early replicating regions (**Fig 2d-f** and **Fig S4c-e**).

ADV aRTIL are closely related to CFSs but are not targeted by DNA damage signalling.

Knowing that CFS are the most sensitive chromosomic regions to RS and that RT delays have been described in these fragile loci, we wondered if ADV aRTIL would also intersect with CFS. To assess the RT changes within CFSs, we analysed the overlaps between aRTIL and already identified CFSs (Brison et al., 2019). We found a clear enrichment of CFS within aRTIL in all 6-cell lines, with 22-44% of CFSs that were located within aRTIL (**Fig 3a-c**). The percentage of CFS containing delayed domains was higher in HCT116, U2OS, MRC5-N and RPE-1 cell line (**Figure 3b**). Quite surprisingly, we showed that CFS localisation was not limited to DEL aRTIL but was also associated to ADV aRTIL, notably for the cancerous RKO and K562 cells. We thus demonstrated that aphidicolin affects CFS replication dynamics, leading to RT delays but also to RT advances.

It has been recently reported that macroH2A1.2, a variant from the canonical H2A (Pehrson and Fried, 1992) having roles both in replication stress response and in cell fate decisions (Barrero et al., 2013; Creppe et al., 2012; Kim et al., 2018a; Pasque et al., 2012) was more abundant at CFSs than non-fragile regions of the genome. In response to aphidicolin treatment, its enrichment is directly correlated with γ-H2AX peak coverage (Kim et al., 2018b).

Using ChiP-seq data from this afore mentioned study, we analysed the coverage of histone variants γ-H2AX and mH2A1.2 in K562 with or without aphidicolin treatment. As we did for the analysis of epigenomic marks, we compared ADV and DEL aRTIL coverage, with Early, Mid and Late replicated regions. First, this result confirms that without aphidicolin, Early-S regions are the most enriched in γ-H2AX and mH2A1.2 histone variants (**Fig 3d-e)** (Seo et al., 2014). As expected, aphidicolin induces a significant increase of γ-H2AX and mH2A1.2 in all control regions. Interestingly, aphidicolin treatment does not modify the coverage of γ-H2AX and mH2A1.2 within ADV aRTIL whereas it induces a strong increase of these two histone modifications coverage within DEL aRTIL (**Fig 3d-e**). This suggests that DEL regions could be very prone to DNA damage under RS, explaining why RT can be delayed in these specific regions. In contrast, ADV aRTIL could be protected from DNA damage or more efficiently repaired, allowing more active replication even under aphidicolin treatment.

Taken together, these results support the fact that, RS can differently affect the RT of fragile regions including CFSs. In contrast to DEL aRTIL, ADV aRTIL were associated to a low level of DNA damage response (DDR) signalling.

Low replication stress impacts the regulation of genes involved in chromatin organization

It has been established that RT switches in human cells can be linked to developmental genes expression (Goren and Cedar, 2003; Hiratani et al., 2004, 2008; Perry et al., 2004). Nonetheless, the exact correlation between RT and gene expression is not entirely clear. Indeed, several studies have discovered genomic sequences that do not fit the general correlation between gene expression and replication timing (Azuara et al., 2003; Gartler, 1999; White et al., 2004). Therefore, we checked if, in our experimental condition, aphidicolin has a global impact on gene expression and if this could explain RT modifications. We performed gene-expression profiling by microarray in RKO cells using the same conditions as for RT analysis. We found that aphidicolin treatment has a mild impact on gene expression, with 14 genes significantly differentially expressed (APH DOWN or APH UP genes) (**Fig 4a and Fig S5a**). When we analysed APH DOWN genes by performing a Gene Ontology (GO) enrichment analysis, we found these genes were enriched in chromatin and nucleosome organization, gene silencing and cellular differentiation pathways (**Fig S5b**). We did not find such enrichment for GO pathways in APH UP genes (FDR > 0.01). Importantly, while the expression of genes that fell inside aRTIL was not affected by low RS, we noticed a general

lower level of gene expression within ADV aRTIL compared to those within DEL aRTIL affected (**Fig 4b**). Altogether, we concluded that while RT modifications under low RS are not related to modification of gene expression within aRTIL, replication stress induces a specific down-regulation of genes involved in chromatin organization.

Aphidicolin modulates chromatin accessibility within ADV aRTIL

Since we found APH DOWN genes in RKO cells involved in chromatin and nucleosome organization, we examine the impact of aphidicolin on chromatin structure by performing ATAC-seq to map chromatin accessibility at the whole-genome level and within specific genomic regions (Buenrostro et al., 2015; Sun et al., 2019). We observed a global decrease of ATAC-seq peaks value under aphidicolin treatment within genomic regions replicating in early or late S phase (**Fig S5c,f**). On the contrary, when we looked at the coverage of ATAC-seq peaks within each region, we observe a global increase (**Fig S5d,f**). Overall, we detected more ATAC-seq peaks, with less intensity, suggesting that there is a global remodelling of chromatin accessibility under aphidicolin treatment. More importantly, we only observed an increase of both ATAC-seq peaks value and coverage within ADV aRTIL while it was not the case within DEL aRTIL (**Fig 4d-e** and **Fig S5e**). Thus we could conclude that under low replication stress chromatin accessibility is specifically increased within ADV aRTIL.

Just like we described that RT modifications were not linked to gene expression, we did not notice increased chromatin accessibility in the UP-transcribed genes (**Fig S5g).** This result indicates that chromatin remodelling and RT modifications induced by aphidicolin during less than a cell cycle treatment duration does not affect gene transcription.

Overall, thanks to this approach, we could conclude that aphidicolin treatment induces a local increase of chromatin accessibility within ADV aRTIL that could be linked to RT modifications while also inducing a whole genome chromatin remodelling.

ADV aRTIL can be transmitted to daughter cells

RT is faithfully reprinted at the beginning of the G1 phase in each cell cycle, at a precise moment named the “timing decision point” or TDP (Dimitrova and Gilbert, 1999; Lu et al., 2010). In G1, RT establishment is dependent on 3D nuclear replication domains organisation through chromatin loop establishment mediated by the Rif1 protein (Foti et al., 2016).

Moreover, at the G1/S transition, chromatin loops are also maintained by the transient recruitment of pre-replication complex proteins and active origins to the nuclear matrix (NM) (Guillou et al., 2010; Lemaitre et al., 2005; Rivera-Mulia et al., 2011; Vogelstein et al., 1980)

We first wondered if RT changes under replication stress in mother cells can be preserved after passage through the G1 phase and thus transmitted to daughter cells. To answer this question, we released the 6 cell lines from aphidicolin or DMSO treatment during the appropriate duration (**Table S2**), and analysed the RT in S phase daughter cells (N+1). Our results indicate that DEL and ADV aRTIL observed in mother cells were no longer detected in the next cell generation of K562, HCT116, U2OS MRC5-N and RPE1 (**Fig 5a and Fig S6a**). In contrast, in RKO cells, the majority (28 of 49) of the strongest and largest ADV aRTIL were transmitted to the next cell generation (**Fig 5a,b** and **Fig S3**) while DEL aRTIL returned to normal RT in daughter cells, comparable to untreated cells. We noticed that the amplitude of RT advances was less pronounced in daughter cells (**Fig 5a** and **Fig S3**), and completely disappeared when cells were analysed after more than three cell cycles following replication stress release (data not shown). These results indicate that while the majority of the RT modifications within aRTIL are reversible and tend to be eliminated through the G1 phase of the next cell cycle, severe ADV aRTIL can be transmitted to the next generation of cells.

To next investigate if the persistence of ADV aRTIL in RKO daughter cells could be linked to changes in chromatin loop organisation in G1 phase, we performed a fluorescent DNA halo experiment to access the extend of the chromatin loops size in G1/S. We used RKO cells as positive control and RPE-1 cells as negative control. We measured the maximum fluorescence Halo radius (MFHR) formed around the nuclear matrix (NM) and noticed a significant shrinkage of DNA loops in the aphidicolin-released RKO cells (**Fig 5c-d**) while no effect was measured in RPE-1 cells (**Fig S6 b-c**). We next wondered if this reduced halo size was correlated to an increase of licensed origins and quantified the loading of pre-replication complex components onto the chromatin in the same conditions. Our results clearly show an increase of MCM2 and p-MCM2 loading onto the chromatin in G1/S of RKO aphidicolin-released daughter cells while it was not the case in RPE-1 cells (Fig S7d), further supporting the DNA halo experiment (**Fig 5e**). Then, the transmission of ADV aRTIL in RKO daughter cells is associated to a decrease in chromatin loop size and an increase of pre-RC proteins loading in G1 phase, predicting more replication origin activation in the next S phase.

Finally, as we observed an effect of chromatin accessibility within ADV aRTIL regions mother cells, we wondered if chromatin remodelling during the passage through the G1 phase

would modulate gene expression within the ADV aRTIL in RKO cells. Even though the expression of genes within ADV aRTIL was not significantly impacted in mother cells, we noticed an up-regulation of genes within ADV aRTIL in daughter cells released from replication stress (**Fig 5f**). We thus performed a gene ontology to see if these ADV aRTIL genes were involved in a specific molecular pathway(s) and we found a strong enrichment for cell-to-cell adhesion and synapse assembly pathways (Fig 5g).

Thus, we could correlate RT advances transmission to differential chromatin remodelling and pre-RC protein loading in G1/S daughter cells further supporting our observation that under replication stress RT advanced are linked to chromatin structure. In addition, we observed that persistence of RT advances in daughter cells is associated to an up-regulation of specific genes. Overall, we revealed that replication stress in mother cells directly affect chromatin accessibility and replication timing that will further affect the cell fate of the next generation.

Discussion

DNA replication is tightly regulated in order to guarantee the accurate passage of genomic information from mother to daughter cells. Challenging structures of DNA are very often encountered by the replication fork and oncogene expression or metabolism changes can also play a deleterious role in DNA replication program efficiency by inducing replication stress. Thus, regardless of the sources, replication stress will give rise to many cellular responses that will depend on the genetic and cellular background of the cell. Importantly, this latest was identified at the early stage of cell transformation and cancer development (Bartkova et al., 2005; Gorgoulis et al., 2005) and persist in cancer cells after the selection steps (Gaillard et al., 2015). As replication stress compromises genome stability, cancer cells have to adapt in order to survive and maintain their proliferation. Due to a high level of genomic instability, cancer cells can lose some of the classical mechanisms involved in DDR, for example through well-known mutations in BRCA1/2 repair genes. However, many compensatory processes take place in cancer cells to allow survival (Bianco et al., 2019; McGrail et al., 2018; Zeman and Cimprich, 2014), also conferring resistance to chemotherapeutic treatments.

In the present work, we demonstrated that one of the components of the replication program, RT, is affected in response to low doses of aphidicolin. Besides the already described

DNA replication delays induced by the replicative DNA polymerases alpha, delta and epsilon inhibition we reveal here that aphidicolin also promotes RT advances. In order to understand how the same replication stress induces such opposite effects, we characterized DEL and ADV aRTIL at both genomic and epigenomic levels. DEL aRTIL are normally replicated in the early-middle S phase and harbour many genes and a high number of constitutive origins of replication. These features explain, the increasing probability for replication forks to be affected by aphidicolin treatment and hampered by transcription activity leading to high DNA damage signalling revealed by high level of γ-H2AX and macroH2A1.2. (Fig 3d,e).

ADV aRTIL are mainly observed in RKO and K562 cancer cells even if they are also detected in the other cell lines. ADV aRTIL correspond to heterochromatin late replicated regions with few and poorly expressed genes, low number of constitutive origins and a low coverage of the two DDR histone marks γ-H2AX and mH2A1.2 that are not significantly increased under low replication stress. Interestingly, in RKO cells, we demonstrated an increase in chromatin accessibility in ADV aRTIL that is not linked to higher gene expression in the mother cells. Altogether, these ADV aRTIL features of are consistent with the fact that they are heterochromatin flexible regions which might be resistant to replication stress.

Under low dose of aphidicolin, the decrease of DNA replication fork velocity can be compensated by the firing of dormant origins, preventing under-replication (Alver et al., 2014; Courbet et al., 2008; Courtot et al., 2018; Ibarra et al., 2008; McIntosh and Blow, 2012; Shima and Pederson, 2017). Interestingly, it was demonstrated in cancer cells that replication origin usage is more flexible (Valenzuela et al., 2012). Moreover, they rely on a higher rate of origin licensing protein expression (McNairn and Gilbert, 2005; Paola and Zannis-Hadjopoulos, 2012) allowing a more efficient dormant origin usage in response to replication stress (Zimmerman et al., 2013). Taking our data into consideration, we can imagine that, in cancer cells, the higher chromatin accessibility described within ADV aRTIL favours the access of DNA replication and repair proteins to these specific heterochromatin regions, leading to dormant origin activation and earlier DNA replication. It was described that replication stress-induced dormant origin activation within a given S phase can be persistent in the next S phase (Courbet et al., 2008). This last result is consistent with our data in RKO cells in which we still observe RT advances in daughter cells after aphidicolin release but also a reduction of DNA halo size and an increase in MCMs loading to chromatin at the G1/S transition. Taken together, these data indicate that some cancer cells are able to modify their replication program and display

a higher flexibility of chromatin organisation and replication origin usage in order to respond to replication stress.

In addition, we observed that genes within ADV aRTIL are up-regulated in daughter cells. These results would suggest that the chronic replication stress described during the first step of cancer development could be involved in the acquisition of replication timing modifications that subsequently lead to changes in the transcription level of specific genes. Altogether, our data indicate that, low RS would change cell fate of cancer cells whose chromatin is more flexible.

RT modifications are historically associated with organism development and cellular differentiation (Hiratani et al., 2008; Nozaki et al., 2017; Pope et al., 2010; Rivera-Mulia et al., 2015). Furthermore, the pluripotent capacity of mammalian cells has been linked to genome plasticity (Hulke et al., 2019; Meshorer et al., 2006) as well as deficiency in Lamin A protein expression (Bronshtein et al., 2015; Ranade et al., 2019). In our study, we observed that RS induced higher level of RT modifications in cancer cells. Interestingly, we showed that RT of the cancerous RKO cell line is strongly affected by aphidicolin treatment inducing major ADV aRTILs. We linked this particular phenotype to the poorly differentiated status of RKO cells together with a very low expression of Lamin A/C (**Table S1**, **Fig S7**). In agreement with this, we noticed that the K562 cell line that had an aRTIL signature close to the RKO cells also expressed a low level of Lamin A/C and it is poorly differentiated (**Table S1, Fig S7**). Overall, we can suggest that the less differentiated cancer cells are, the more they will harbour RT advances in response to replication stress.

Finally, this study unveiled a new mechanism in response to replication stress that may have strong consequences on gene expression and cellular identity, mainly for cancer cells. It would be hugely relevant to further investigate the molecular actors playing to advance replication timing in cancer cells as it could lead to the identification of potential new targets to impede cancer cells adaptation to replication stress.

Material and method

Cell lines, cell culture and drugs

The 6 human cell lines were purchased from ATCC. Cells were grown in culture medium supplemented with 10% fetal bovine serum (Gibco Life Technologies A31608-02) at 37°C, 5% CO2 and 5% O2. HCT116, U2OS and RKO cell lines were grown in Dulbecco's Modified Eagle's Medium (DMEM, Gibco Life Technologies 31966021), MRC5-N cell line was grown in Minimum Essential Medium Eagle (MEM-aplha, Gibco Life Technologies 22561021), RPE-1 cell line was grown in Roswell Park Memorial Institute Media (RPMI, Gibco Life Technologies 61870044) and K562 in Iscove Modified Dulbecco Media (IMDM, Gibco Life Technologies 21980032) supplemented with decomplemented serum. Aphidicolin (Sigma-Aldrich AO781-1MG) stock solution was diluted in DMSO (Sigma-Aldrich D8418-250mL) and kept at -20°C for a maximum of 2 months after first thawing. Cells were synchronized in G1/S with 0.5mM L-Mimosine (Sigma-Aldrich M0253) for 24h.

Fluorescence Activated Cell Sorting (FACS)

Cells were pulse-labelled with 10µM BrdU and/or EdU for indicated times then collected by trypsinization and fixed in 70% ice-cold ethanol overnight at −20°C. For EdU and BrdU immunodetection, we followed the protocol described on (Bradford and Clarke, 2011). Finally, after washing in PBS–BSA 0.5%, then in PBS, cells were resuspended in PBS with propidium iodide (25 µg/mL, Sigma-Aldrich) and RNase A (100 µg/mL, Thermo Fisher Scientific) or with DAPI (1/1000, Sigma-Aldrich, D9542). After 20 min of incubation at room temperature, cell cycle analysis was carried out by flow cytometry with a MACSQuant 10 or VYB cytometer (Miltenyi Biotec) and analysed with FlowLogic software.

Cell lysis, fractionation and western blotting

For whole cell extract, cells were lysed for 30min on ice with classic lysis buffer (0.3M NaCl, 1% triton, 50mM Tris pH7.5, 5mM EDTA, 1mM DTT and 1X Halt protease and phosphatase inhibitor cocktail from Thermo Fisher Scientific 78445).

For subcellular fractionation, cells were lysed in Buffer A (Hepes 10mM pH 7.9, KCl 10mM, MgCl2 1.5mM, sucrose 0.34M, Glycerol 10%, dithiothreitol (DTT) 1mM, 1X Halt protease and

phosphatase inhibitor cocktail) complemented with Triton X-100 0.1% for 5min on ice. After centrifugation at 1,500rcf, 5min, 4°C, the supernatant was clarified by high-speed centrifugation (18,000rcf, 4°C, 15min) to obtain the cytoplasmic fraction. The pellet was washed once with Buffer A and then incubated in Buffer B (EDTA 3.2mM, DTT 1mM, Halt protease and phosphatase inhibitor cocktail) for 30min on ice. After centrifugation (1,700rcf, 5min, 4°C), the supernatant was collected as the soluble nuclear fraction. The pellet (chromatin fraction) was washed once with Buffer B and resuspended in the same buffer. The whole cell extracts and chromatin-enriched fractions were then sonicated (10 pulses of 1s at 40% amplitude with a Sonics Vibra Cell Ultrasonic processor) and Laemmli buffer was added in order to have a final protein concentration of 2µg/µL and 0.5µg/µL respectively. The detection of pChk1 (S345, Cell signalling, Rabbit), Chk1 (Santa Cruz, Mouse), Actinin (MBL, Mouse), MCM2 (Abcam, Rabbit), p-MCM2 (Abcam, Rabbit), ORC2 (MBL, Mouse) Lamin A/C (Santa cruz, Mouse) and Tubulin (Genetex, Mouse) was done by running SDS-page gels, transferring on PVDF membranes, blocking with 5%milk, incubating with primary antibody (in TBS-T, adapted dilutions) followed by secondary antibody (MBL, Mouse or Rabbit, 1/10 000 in TBS-T) and finally revealing thanks to ECL (Biorad) under the ChemiDoc imaging system (BioRad)

Replication timing analysis

10-20M exponentially growing mammalian cells (with DMSO or aphidicolin) were incubated with 0.5mM BrdU (Abcam, #142567), protected from light, at 37°C for 90 minutes. After washing in PBS, cells were fixed in 75% final cold EtOH and stored at -20°C. BrdU labeled cells were incubated with 80µg/mL Propidium Iodide (Invitrogen, P3566) and with 0,4 mg/ml RNaseA (Roche, 10109169001) for 15min at room temperature and 150 000 cells were sorted in early (S1) and late (S2) S phase fractions using a Fluorescence Activated Cell Sorting system (FACSAria Fusion, Becton Dickinson) in Lysis Buffer (50mM Tris pH=8, 10mM EDTA, 0.5% SDS, 300mM NaCl) and stored at -20°C until the following steps. DNA from S1 and S2 fractions of sorted cells was extracted using Proteinase K treatment (200µg/ml, Thermo Scientific, EO0491) followed by phenol-chloroform extraction and sonicated to a size of 500-1,000 base pair (bp), as previously described (Hadjadj et al., 2016). Immunoprecipitation was performed using IP star robot at 4°C (indirect 200µl method, SX-8G IP-Star® Compact Automated System, Diagenode) with an anti-BrdU antibody (10µg, purified mouse Anti-BrdU, BD Biosciences, #347580). Denatured DNA was incubated 5 hours with anti-BrdU antibodies in IP buffer

(10mM Tris pH=8, 1mM EDTA, 150mM NaCl, 0.5% Triton X-100, 7mM NaOH) followed by an incubation of 5 hours with Dynabeads Protein G (Invitrogen, 10004D). Beads were then washed with Wash Buffer (20mM Tris pH=8, 2mM EDTA, 250mM NaCl, 1% Triton X-100). Reversion was performed at 37°C during 2 hours with a solution containing 1% SDS and 0.5mg Proteinase K followed, after the beads removal, by an incubation at 65°C during 6 hours in the same solution. Immunoprecipitated BrdU labeled DNA fragments were extracted with phenol-chloroform and precipitated with cold ethanol. Control quantitative PCRs (qPCRs) were performed using oligonucleotides specific of mitochondrial DNA, early (BMP1 gene) or late (DPPA2 gene) replicating regions (Ryba et al., 2011; Hadjadj et al., 2016). Whole genome amplification was performed using SeqPlextm Enhanced DNA Amplification kit as described by the manufacturer (Sigma-Aldrich, SEQXE). Amplified DNA was purified using PCR purification product kit as described by the manufacturer (Macherey-Nagel, 740609.50). DNA amount was measured using a Nanodrop. Quantitative PCRs using the oligonucleotides described above were performed to check whether the ratio between early and late replication regions was still maintained after amplification. Early and late nascent DNA fractions were labelled with Cy3-ULS and Cy5-ULS, respectively, using the ULS arrayCGH labeling Kit (Kreatech, EA-005). Same amounts of early and late-labeled DNA were loaded on human DNA microarrays (SurePrint G3 Human CGH arrays, Agilent Technologies, G4449A). Hybridization was performed as previously described (Hadjadj et al., 2016). The following day, microarrays were scanned using an Agilent C-scanner with Feature Extraction 9.1 software (Agilent technologies). To determine the replication domains and do the comparative analysis in different conditions, the online platform specific for replication timing data START-R (Hadjadj et al., 2020) was used, with biological duplicates for each condition. The output bed file gave the list of significantly impacted genomic regions (ADVANCED or DELAYED) and the report of number and percentage of genomic regions impacted. We also used the output replication timing smooth files to stratify the early (RT > 1) the mid (-1 < RT < 1) and late (RT < -1) replicating regions.

BrdU ChiP-qPCR

The same protocol as for replication timing was performed until BrdU immunoprecipitation (IP). For the BrdU-IP, 140µL of IP buffer (Tris pH8 50mM, EDTA 2mM, NaCl 300mM, Triton 1%, H2O qsp, 14mM NaOH extemporaneously) and 40µL of the monoclonal anti-BrdU antibody (BD Biosciences, 347580) were added to DNA and incubated on rotating wheel overnight at

4°C. 50µL of magnetic beads (Dynabeads™ Protein G, Thermofisher) previously washed with PBS (15min on wheel at RT) and IP buffer was added to the mix and incubated on wheel 2 hours at 4°C. After washing twice with 800µL of Buffer B (Tris pH8 20mM, EDTA 2mM, NaCl 250mM, Triton 0.2%, H2O qsp) and with 800µL of Tris pH8 10mM, beads were resuspended in 100µL of Tris pH8 10mM. Immuno-precipitated DNA was then recovered by a reversion step with SDS1% and PK 20mg/mL 2h at 37°C on shaking. Supernatant was incubated overnight at 65°C on shaking. A final phenol-chloroform purification was performed and DNA concentration was measured with Nanodrop technology before performing qPCR. For the qPCR experiment, 2µL BrdU-IP-DNA, was added to a mix of 4.5µL H2O, 7.5µL of primer couple (**Table S4**) and 6µL of SYBR Green (Master Mix, Thermofisher) on 96 well plate. For each primer couple a DNA concentration scale (0.0325, 0.125, 0.5, 2ng/µL) was performed. StepOne technology was used to do the qPCR with a classical run of 2 hours. For each genomic region amplified, we quantified the percentage of S1 and S2 after normalization with mitochondrial DNA.

RNA-ChiP

Exponentially growing cells (with DMSO or aphidicolin) were harvested and RNAs were extracted with RNeasy plus mini kit (Qiagen). RNAs quality and quantity were controlled using Nanodrop ND-1000 and Bioanalyzer 2100 Expert from Agilent. cDNAs were prepared according to the standard ThermoFisher protocol from 100ng total RNA (GeneChip™ WT PLUS Reagent Kit Manual Target Preparation for GeneChip™ Whole Transcript (WT) Expression Arrays User Guide). Following fragmentation, 5.5 ug of single stranded cDNA were hybridized on Human Clariom S Arrays in GeneChip Hybridization Oven 645 for 16 hr at 45°C. The arrays were washed and stained in the Affymetrix Fluidics Station 450. Arrays were scanned using the GeneChip Scanner GC3000 7G and images were analysed using Command Console software to obtain the raw data (values of fluorescent intensity). The data were analysed with TAC (Transcriptome Analysis Console, version 4.0.2.15) from ThermoFisher. Microarrays were normalized with the “Robust Multichip Analysis” (SST-RMA) method. Statistical analysis allowed tagging of genes according to the fold change (FC) and the p-value adjusted together with ANOVA approach.

ATAC-seq

100 000 exponentially growing RKO cells were trypsinized, washed in PBS and treated with 1:100 volume of RNase-free DNase (QIAGEN) and DMEM media during 30min at 37°C in the incubator. Cells were trypsynized, washed in PBS and resuspended in 500µL of ice-cold crypreservation solution (50% FBS, 40% DMEM, 10% DMSO), transferred into a 2mL cryotubes and frozed in a pre-chilled Mr. Frosty container at -80°C overnight or more before sending to Active Motif to perform ATAC-seq assay. The cells were then thawed in a 37°C water bath, pelleted, washed with cold PBS, and tagmented as previously described (Buenrostro et al., 2013), with some modifications based on (Corces et al., 2017). Briefly, cell pellets were resuspended in lysis buffer, pelleted, and tagmented using the enzyme and buffer provided in the Nextera Library Prep Kit (Illumina). Tagmented DNA was then purified using the MinElute PCR purification kit (Qiagen), amplified with 10 cycles of PCR, and purified using Agencourt AMPure SPRI beads (Beckman Coulter). Resulting material was quantified using the KAPA Library Quantification Kit for Illumina platforms (KAPA Biosystems), and sequenced with PE42 sequencing on the NextSeq 500 sequencer (Illumina). Analysis of ATAC-seq data was very similar to the analysis of ChIP-Seq data. Reads were aligned using the BWA algorithm (mem mode; default settings). Duplicate reads were removed, only reads mapping as matched pairs and only uniquely mapped reads (mapping quality >= 1) were used for further analysis. Alignments were extended in silico at their 3'-ends to a length of 200 bp and assigned to 32-nt bins along the genome. The resulting histograms (genomic "signal maps") were stored in bigWig files. Peaks were identified using the MACS 2.1.0 algorithm at a cutoff of p-value 1e-7, without control file, and with the –nomodel option. Peaks that were on the ENCODE blacklist of known false ChIP-Seq peaks were removed. Signal maps and peak locations were used as input data to Active Motifs proprietary analysis program, which creates Excel tables containing detailed information on sample comparison, peak metrics, peak locations and gene annotations. To then annotate the ATAC-seq peak value and coverage within genomic regions of interest, we used Merge BedGraph and AnnotateBed bedtools functions respectively (Galaxy Version 2.29.2). We then normalized the three biological replicates values regarding all genomic regions (Early, Mid, Late, ADV and DEL) by a 2way ANOVA Sidak's multiple comparisons test.

Processing ChiP-seq data from public databases

ChiP-seq, pDamID and RepOri data were download from ENCODE, GEO, 4DN project and Replication domain data base respectively (**Table S5**). The epigenetic marks coverage of each given regions list (Early, Mid, Late, ADV, DEL) was calculated using AnnotatedBed bedtools function (Galaxy Version 2.29.2). The mean for each epigenetic mark coverage in given regions was calculated to generate clustering tree heatmap based on Pearson correlations with ClustVis software (Metsalu and Vilo, 2015).

DNA Halos experiment

400 000 cells were harvested after synchronization and treated with nuclei buffer (10 mM Tris at pH 8, 3 mM MgCl2, 0.1 M NaCl, 0.3 M sucrose, protease inhibitors) plus 0.5% Nonidet P40 for 5-10 min on ice (depending on cell line). Nuclei were attached to coverslips using cytospin (1500-1800 rpm for 5-10 min, depending on cell line); stained with 2 mg/mL DAPI for 4 min; and immersed in a buffer containing 25 mM Tris (pH 8), 0.5 M NaCl, 0.2 mM MgCl2, 1 mM PMSF, and protease inhibitors for 1 min, then in Halo Buffer (10 mM Tris at pH 8, 2 M NaCl, 10 mM ethylene diamine tetra acetic acid [EDTA], 1 mM DTT, protease inhibi- tors) for 4 min. After two washing steps with wash buffer 1 (25 mM Tris (pH 8), 0.2 M NaCl, and 0.2 mM MgCl2) for 1 min, and was buffer 2 (buffer 1 without NaCl) for 1 min extracted nuclei were fixed in 2% formaldehyde for 10 min and processed for immunofluorescence. Images containing about 200 Halo per condition were taken with a Nikon Ni-E microscope and a DS-Qi2 camera with 64X objective and MFHR (Maximum Fluorescence Halo Radius) was measured in Image J software.

Acknowledgments:

Fundings: Ligue nationale contre le cancer, Institut National du Cancer (INCA), Centre de Recherches en Cancérologie de Toulouse (CRCT) and Fondation pour la Recherche Médicale (FRM).

Technical facilities: We gratefully acknowledge the Technologic platform from CRCT (Manon Farcé for cytometry, Marie Tosolini and Juan-Pablo Cerapio-Arroyo for the bio-informatics analysis). The authors also thank Nathalie Marsaud (GeT-Biopuces, Toulouse Biochip Facility) for help and advice about the experimental protocol of Microarray Transcriptomic.

Personal Acknowledgments: V.B. and L.C. personally want to thank Gaëlle Legube, Vincent Rocher, Marie Jeanne Pillaire and Guillaume Labrousse for their helpful advices and discussions all along this project. We want also to thank Sarah McClelland, Laure Crabbe and Jean-Yves Masson, for their precious feedbacks and proofreading.

Bibliography

Almeida, R., Fernández-Justel, J.M., Santa-María, C., Cadoret, J.-C., Cano-Aroca, L., Lombraña, R., Herranz, G., Agresti, A., and Gómez, M. (2018). Chromatin conformation regulates the coordination between DNA replication and transcription. Nat. Commun. 9, 1590.

Arlt, M.F., Casper, A.M., and Glover, T.W. (2003). Common fragile sites. Cytogenet. Genome Res. 100, 92–100.

Azuara, V., Brown, K.E., Williams, R.R.E., Webb, N., Dillon, N., Festenstein, R., Buckle, V., Merkenschlager, M., and Fisher, A.G. (2003). Heritable gene silencing in lymphocytes delays chromatid resolution without affecting the timing of DNA replication. Nat. Cell Biol. 5, 668–674.

Barrero, M.J., Sese, B., Kuebler, B., Bilic, J., Boue, S., Martí, M., and Izpisua Belmonte, J.C. (2013). Macrohistone Variants Preserve Cell Identity by Preventing the Gain of H3K4me2 during Reprogramming to Pluripotency. Cell Rep. 3, 1005–1011.

Berezney, R., Dubey, D.D., and Huberman, J.A. (2000). Heterogeneity of eukaryotic replicons, replicon clusters, and replication foci. Chromosoma 108, 471–484.

Bradford, J.A., and Clarke, S.T. (2011). Dual-pulse labeling using 5-ethynyl-2'-deoxyuridine (EdU) and 5-bromo-2'-deoxyuridine (BrdU) in flow cytometry. Curr. Protoc. Cytom. Chapter 7, Unit 7.38.

Brison, O., El-Hilali, S., Azar, D., Koundrioukoff, S., Schmidt, M., Nähse, V., Jaszczyszyn, Y., Lachages, A.-M., Dutrillaux, B., Thermes, C., et al. (2019). Transcription-mediated organization of the replication initiation program across large genes sets common fragile sites genome-wide. Nat. Commun. 10, 5693.

Buenrostro, J., Wu, B., Chang, H., and Greenleaf, W. (2015). ATAC-seq: A Method for Assaying Chromatin Accessibility Genome-Wide. Curr. Protoc. Mol. Biol. Ed. Frederick M Ausubel Al 109, 21.29.1-21.29.9.

Buenrostro, J.D., Giresi, P.G., Zaba, L.C., Chang, H.Y., and Greenleaf, W.J. (2013). Transposition of native chromatin for fast and sensitive epigenomic profiling of open chromatin, DNA-binding proteins and nucleosome position. Nat. Methods 10, 1213–1218.

Chan, K.L., Palmai-Pallag, T., Ying, S., and Hickson, I.D. (2009). Replication stress induces sister-chromatid bridging at fragile site loci in mitosis. Nat. Cell Biol. 11, 753–760.

Corces, M.R., Trevino, A.E., Hamilton, E.G., Greenside, P.G., Sinnott-Armstrong, N.A., Vesuna, S., Satpathy, A.T., Rubin, A.J., Montine, K.S., Wu, B., et al. (2017). An improved ATAC-seq protocol reduces background and enables interrogation of frozen tissues. Nat. Methods 14, 959–962.

Creppe, C., Janich, P., Cantariño, N., Noguera, M., Valero, V., Musulén, E., Douet, J., Posavec, M., Martín-Caballero, J., Sumoy, L., et al. (2012). MacroH2A1 regulates the balance between self-renewal and differentiation commitment in embryonic and adult stem cells. Mol. Cell. Biol. 32, 1442–1452.

Dimitrova, D.S., and Gilbert, D.M. (1999). The Spatial Position and Replication Timing of Chromosomal Domains Are Both Established in Early G1 Phase. Mol. Cell 4, 983–993.

Donley, N., and Thayer, M.J. (2013). DNA replication timing, genome stability and cancer. Semin. Cancer Biol. 23, 80–89.

Fernandez-Vidal, A., Guitton-Sert, L., Cadoret, J.-C., Drac, M., Schwob, E., Baldacci, G., Cazaux, C., and Hoffmann, J.-S. (2014). A role for DNA polymerase θ in the timing of DNA replication. Nat. Commun. 5, 1–10.

Foti, R., Gnan, S., Cornacchia, D., Dileep, V., Bulut-Karslioglu, A., Diehl, S., Buness, A., Klein, F.A., Huber, W., Johnstone, E., et al. (2016). Nuclear Architecture Organized by Rif1 Underpins the Replication-Timing Program. Mol. Cell 61, 260–273.

Gartler, S. (1999). The timing of XIST replication: dominance of the domain. Hum. Mol. Genet. 8, 1085–1089.

Gómez-González, B., and Aguilera, A. (2019). Transcription-mediated replication hindrance: a major driver of genome instability. Genes Dev. 33, 1008–1026.

Goren, A., and Cedar, H. (2003). Replicating by the clock. Nat. Rev. Mol. Cell Biol. 4, 25–32.

Gorgoulis, V.G., Vassiliou, L.-V.F., Karakaidos, P., Zacharatos, P., Kotsinas, A., Liloglou, T., Venere, M., DiTullio, R.A., Kastrinakis, N.G., Levy, B., et al. (2005). Activation of the DNA damage checkpoint and genomic instability in human precancerous lesions. Nature 434, 907–913.

Guillou, E., Ibarra, A., Coulon, V., Casado-Vela, J., Rico, D., Casal, I., Schwob, E., Losada, A., and Méndez, J. (2010). Cohesin organizes chromatin loops at DNA replication factories. Genes Dev. 24, 2812–2822.

Hadjadj, D., Denecker, T., Maric, C., Fauchereau, F., Baldacci, G., and Cadoret, J.-C. (2016). Characterization of the replication timing program of 6 human model cell lines. Genomics Data 9, 113–117.

Hadjadj, D., Denecker, T., Guérin, E., Kim, S.-J., Fauchereau, F., Baldacci, G., Maric, C., and Cadoret, J.-C. (2020). Efficient, quick and easy-to-use DNA replication timing analysis with START-R suite. NAR Genomics Bioinforma. 2.

Harrigan, J.A., Belotserkovskaya, R., Coates, J., Dimitrova, D.S., Polo, S.E., Bradshaw, C.R., Fraser, P., and Jackson, S.P. (2011). Replication stress induces 53BP1-containing OPT domains in G1 cells. J. Cell Biol. 193, 97–108.

Hecht, F., and Glover, T.W. (1984). Cancer chromosome breakpoints and common fragile sites induced by aphidicolin. Cancer Genet. Cytogenet. 13, 185–188.

Hiratani, I., Leskovar, A., and Gilbert, D.M. (2004). Differentiation-induced replication-timing changes are restricted to AT-rich/long interspersed nuclear element (LINE)-rich isochores. Proc. Natl. Acad. Sci. 101, 16861–16866.

Hiratani, I., Ryba, T., Itoh, M., Yokochi, T., Schwaiger, M., Chang, C.-W., Lyou, Y., Townes, T.M., Schübeler, D., and Gilbert, D.M. (2008). Global Reorganization of Replication Domains During Embryonic Stem Cell Differentiation. PLOS Biol. 6, e245.

Hiratani, I., Ryba, T., Itoh, M., Rathjen, J., Kulik, M., Papp, B., Fussner, E., Bazett-Jones, D.P., Plath, K., Dalton, S., et al. (2010). Genome-wide dynamics of replication timing revealed by in vitro models of mouse embryogenesis. Genome Res. 20, 155–169.

Jackson, D.A., and Pombo, A. (1998). Replicon Clusters Are Stable Units of Chromosome Structure: Evidence That Nuclear Organization Contributes to the Efficient Activation and Propagation of S Phase in Human Cells. J. Cell Biol. 140, 1285–1295.

Ji, F., Liao, H., Pan, S., Ouyang, L., Jia, F., Fu, Z., Zhang, F., Geng, X., Wang, X., Li, T., et al. (2020). Genome-wide high-resolution mapping of mitotic DNA synthesis sites and common fragile sites by direct sequencing. Cell Res.

Jones, R.M., Mortusewicz, O., Afzal, I., Lorvellec, M., García, P., Helleday, T., and Petermann, E. (2013). Increased replication initiation and conflicts with transcription underlie Cyclin E-induced replication stress. Oncogene 32, 3744–3753.

Julienne, H., Audit, B., and Arneodo, A. (2015). Embryonic stem cell specific "master" replication origins at the heart of the loss of pluripotency. PLoS Comput. Biol. 11, e1003969.

Kim, J., Oberdoerffer, P., and Khurana, S. (2018a). The histone variant macroH2A1 is a splicing-modulated caretaker of genome integrity and tumor growth. Mol. Cell. Oncol. 5, e1441629.

Kim, J., Sturgill, D., Sebastian, R., Khurana, S., Tran, A.D., Edwards, G.B., Kruswick, A., Burkett, S., Hosogane, E.K., Hannon, W.W., et al. (2018b). Replication Stress Shapes a Protective Chromatin Environment across Fragile Genomic Regions. Mol. Cell 69, 36-47.e7.

Kotsantis, P., Petermann, E., and Boulton, S.J. (2018). Mechanisms of Oncogene-Induced Replication Stress: Jigsaw Falling into Place. Cancer Discov. 8, 537–555.

Lemaitre, J.-M., Danis, E., Pasero, P., Vassetzky, Y., and Méchali, M. (2005). Mitotic Remodeling of the Replicon and Chromosome Structure. Cell 123, 787–801.

Le Tallec, B., Millot, G.A., Blin, M.E., Brison, O., Dutrillaux, B., and Debatisse, M. (2013). Common Fragile Site Profiling in Epithelial and Erythroid Cells Reveals that Most Recurrent Cancer Deletions Lie in Fragile Sites Hosting Large Genes. Cell Rep. 4, 420–428.

Letessier, A., Millot, G.A., Koundrioukoff, S., Lachagès, A.-M., Vogt, N., Hansen, R.S., Malfoy, B., Brison, O., and Debatisse, M. (2011). Cell-type-specific replication initiation programs set fragility of the FRA3B fragile site. Nature 470, 120–123.

Lu, J., Li, F., Murphy, C.S., Davidson, M.W., and Gilbert, D.M. (2010). G2 phase chromatin lacks determinants of replication timing. J. Cell Biol. 189, 967–980.

Lukas, C., Savic, V., Bekker-Jensen, S., Doil, C., Neumann, B., Sølvhøj Pedersen, R., Grøfte, M., Chan, K.L., Hickson, I.D., Bartek, J., et al. (2011). 53BP1 nuclear bodies form around DNA lesions generated by mitotic transmission of chromosomes under replication stress. Nat. Cell Biol. 13, 243–253.

Macheret, M., Bhowmick, R., Sobkowiak, K., Padayachy, L., Mailler, J., Hickson, I.D., and Halazonetis, T.D. (2020). High-resolution mapping of mitotic DNA synthesis regions and common fragile sites in the human genome through direct sequencing. Cell Res.

Madrid-Mencía, M., Raineri, E., Cao, T.B.N., and Pancaldi, V. (2020). Using GARDEN-NET and ChAseR to explore human haematopoietic 3D chromatin interaction networks. Nucleic Acids Res. 48, 4066–4080.

Magdalou, I., Lopez, B.S., Pasero, P., and Lambert, S.A.E. (2014). The causes of replication stress and their consequences on genome stability and cell fate. Semin. Cell Dev. Biol. 30, 154–164.

Masai, H., Matsumoto, S., You, Z., Yoshizawa-Sugata, N., and Oda, M. (2010). Eukaryotic Chromosome DNA Replication: Where, When, and How? Annu. Rev. Biochem. 79, 89–130.

Metsalu, T., and Vilo, J. (2015). ClustVis: a web tool for visualizing clustering of multivariate data using Principal Component Analysis and heatmap. Nucleic Acids Res. 43, W566–W570.

Miron, K., Golan-Lev, T., Dvir, R., Ben-David, E., and Kerem, B. (2015). Oncogenes create a unique landscape of fragile sites. Nat. Commun. 6, 7094.

Naim, V., and Rosselli, F. (2009). The FANC pathway and BLM collaborate during mitosis to prevent micro-nucleation and chromosome abnormalities. Nat. Cell Biol. 11, 761–768.

Ozeri-Galai, E., Bester, A.C., and Kerem, B. (2012). The complex basis underlying common fragile site instability in cancer. Trends Genet. 28, 295–302.

Pasque, V., Radzisheuskaya, A., Gillich, A., Halley-Stott, R.P., Panamarova, M., Zernicka-Goetz, M., Surani, M.A., and Silva, J.C.R. (2012). Histone variant macroH2A marks embryonic differentiation in vivo and acts as an epigenetic barrier to induced pluripotency. J. Cell Sci. 125, 6094–6104.

Pehrson, J.R., and Fried, V.A. (1992). MacroH2A, a core histone containing a large nonhistone region. Science 257, 1398–1400.

Perry, P., Sauer, S., Billon, N., Richardson, W.D., Spivakov, M., Warnes, G., Livesey, F.J., Merkenschlager, M., Fisher, A.G., and Azuara, V. (2004). A dynamic switch in the replication timing of key regulator genes in embryonic stem cells upon neural induction. Cell Cycle Georget. Tex 3, 1645–1650.

Pope, B.D., Hiratani, I., and Gilbert, D.M. (2010). Domain-wide regulation of DNA replication timing during mammalian development. Chromosome Res. 18, 127–136.

Rivera-Mulia, J.C., Hernández-Muñoz, R., Martínez, F., and Aranda-Anzaldo, A. (2011). DNA moves sequentially towards the nuclear matrix during DNA replication in vivo. BMC Cell Biol. 12, 3.

Rivera-Mulia, J.C., Buckley, Q., Sasaki, T., Zimmerman, J., Didier, R.A., Nazor, K., Loring, J.F., Lian, Z., Weissman, S., Robins, A.J., et al. (2015). Dynamic changes in replication timing and gene expression during lineage specification of human pluripotent stem cells. Genome Res. 25, 1091–1103.

Rivera-Mulia, J.C., Desprat, R., Trevilla-Garcia, C., Cornacchia, D., Schwerer, H., Sasaki, T., Sima, J., Fells, T., Studer, L., Lemaitre, J.-M., et al. (2017). DNA replication timing alterations identify common markers between distinct progeroid diseases. Proc. Natl. Acad. Sci. 114, E10972–E10980.

Rivera-Mulia, J.C., Sasaki, T., Trevilla-Garcia, C., Nakamichi, N., Knapp, D.J.H.F., Hammond, C.A., Chang, B.H., Tyner, J.W., Devidas, M., Zimmerman, J., et al. (2019). Replication timing alterations in leukemia affect clinically relevant chromosome domains. Blood Adv. 3, 3201–3213.

Ryba, T., Hiratani, I., Lu, J., Itoh, M., Kulik, M., Zhang, J., Schulz, T.C., Robins, A.J., Dalton, S., and Gilbert, D.M. (2010). Evolutionarily conserved replication timing profiles predict long-range chromatin interactions and distinguish closely related cell types. Genome Res. 20, 761–770.

Ryba, T., Hiratani, I., Sasaki, T., Battaglia, D., Kulik, M., Zhang, J., Dalton, S., and Gilbert, D.M. (2011). Replication Timing: A Fingerprint for Cell Identity and Pluripotency. PLoS Comput. Biol. 7, e1002225.

Ryba, T., Battaglia, D., Chang, B.H., Shirley, J.W., Buckley, Q., Pope, B.D., Devidas, M., Druker, B.J., and Gilbert, D.M. (2012). Abnormal developmental control of replication-timing domains in pediatric acute lymphoblastic leukemia. Genome Res. 22, 1833–1844.

Sarni, D., Sasaki, T., Irony Tur-Sinai, M., Miron, K., Rivera-Mulia, J.C., Magnuson, B., Ljungman, M., Gilbert, D.M., and Kerem, B. (2020). 3D genome organization contributes to genome instability at fragile sites. Nat. Commun. 11, 3613.

Seo, J., Kim, K., Chang, D.-Y., Kang, H.-B., Shin, E.-C., Kwon, J., and Choi, J.K. (2014). Genome-wide reorganization of histone H2AX toward particular fragile sites on cell activation. Nucleic Acids Res. 42, 1016–1025.

Sun, Y., Miao, N., and Sun, T. (2019). Detect accessible chromatin using ATAC-sequencing, from principle to applications. Hereditas 156.

Takahashi, S., Miura, H., Shibata, T., Nagao, K., Okumura, K., Ogata, M., Obuse, C., Takebayashi, S., and Hiratani, I. (2019). Genome-wide stability of the DNA replication program in single mammalian cells. Nat. Genet. 51, 529–540.

Vogelstein, B., Pardoll, D.M., and Coffey, D.S. (1980). Supercoiled loops and eucaryotic DNA replication. Cell 22, 79–85.

White, E.J., Emanuelsson, O., Scalzo, D., Royce, T., Kosak, S., Oakeley, E.J., Weissman, S., Gerstein, M., Groudine, M., Snyder, M., et al. (2004). DNA replication-timing analysis of human chromosome 22 at high resolution and different developmental states. Proc. Natl. Acad. Sci. 101, 17771–17776.

Wilson, T.E., Arlt, M.F., Park, S.H., Rajendran, S., Paulsen, M., Ljungman, M., and Glover, T.W. (2015). Large transcription units unify copy number variants and common fragile sites arising under replication stress. Genome Res. 25, 189–200.

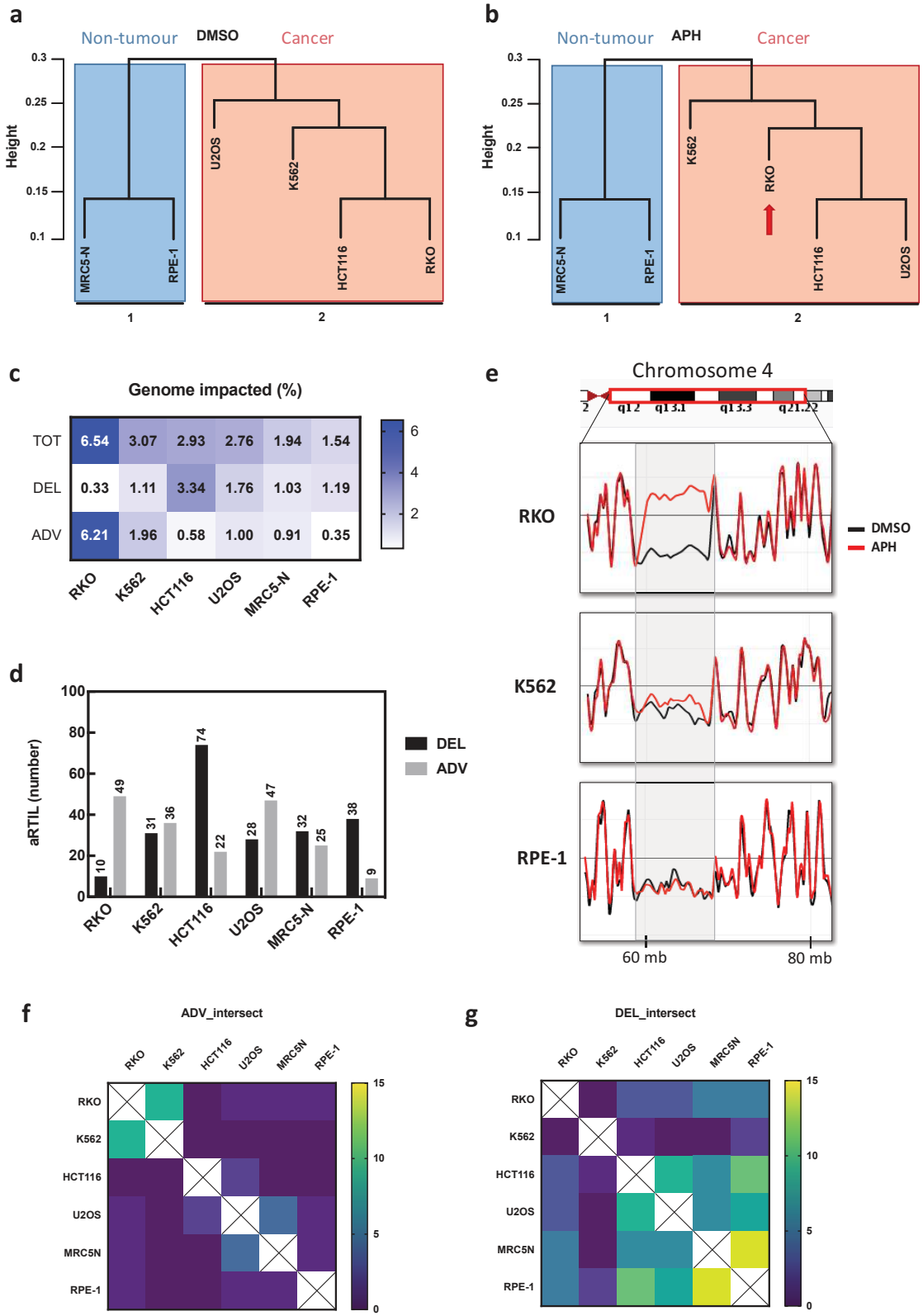

Figure 1: Low replication stress differentially impacts cancer and normal cells. a Cluster dendogram based on p-values reflecting on RT signatures in DMSO condition of the six cell lines. Distance: correlation and clustering method: average. **b** Cluster dendogram based on p-values reflecting on RT signatures in APH condition of the six cell lines. Distance: correlation and clustering method: average. **c** Heatmap representing the coverage (in % of the genome) of impacted genomic regions: total, delayed or advanced (TOT, DEL and ADV) for each cell line. **d** Quantification of the number of genomic regions significantly impacted (DEL, black and ADV

in grey) by aphidicolin treatment. **e** Screenshot of Loess-smooth RT profiles for the same region in chromosome 4 for RKO, K562 and RPE-1 cells. The dark lines correspond to replication timing of control (DMSO) replication timing (2 independent replicates) and the red lines are replication timing of APH treated cells (2 independent replicates). **f** Heatmap with intersections (the sum of the number of common domains) for ADV genomic regions between cell lines. **g** Heatmap with intersections (the sum of the number of common domains) for DEL genomic regions between cell lines.

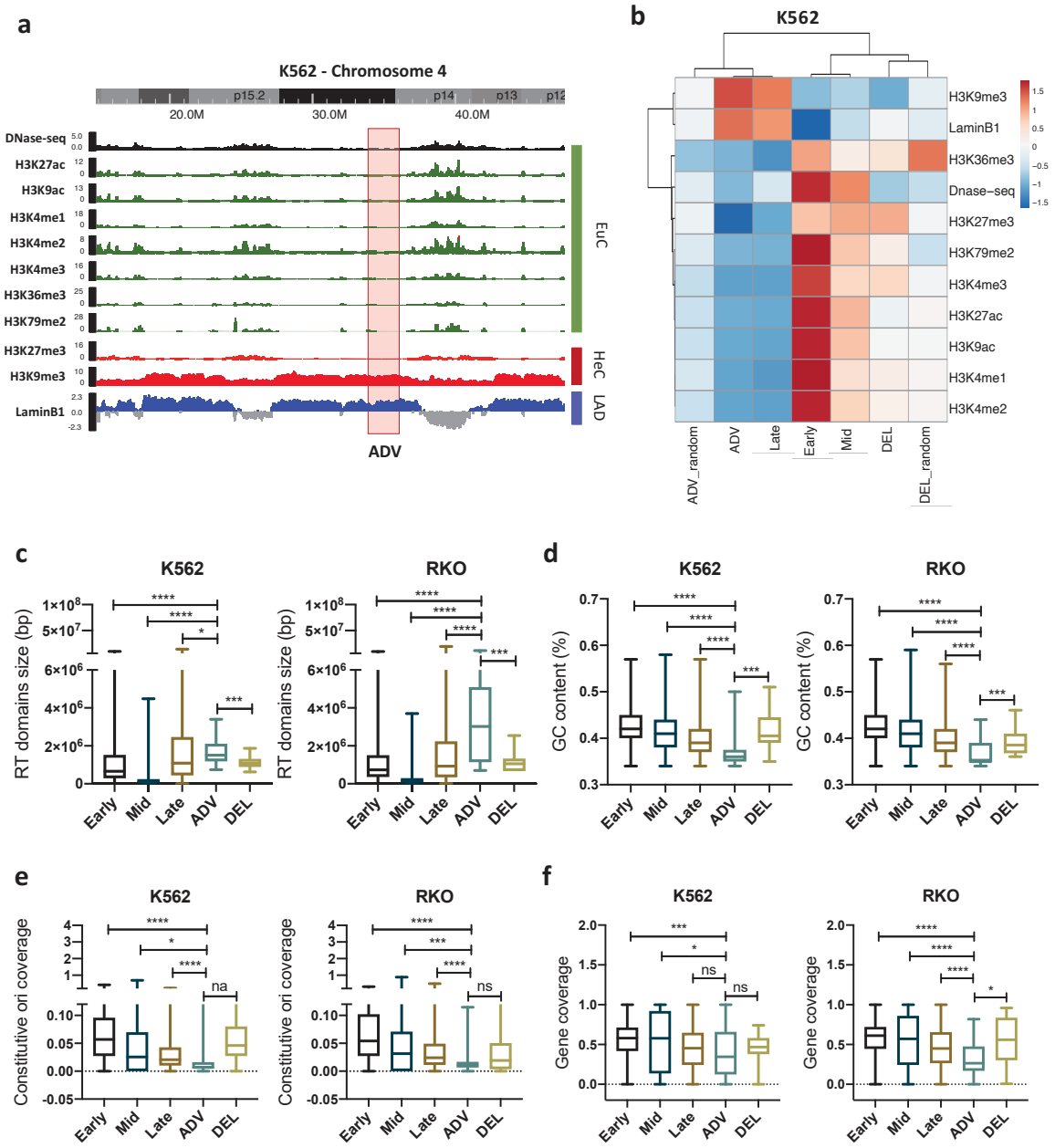

<u>Figure 2:</u> ADV aRTIL are housed in heterochromatin late replicated chromosomic regions. a Screenshot of WashUEpigenome Browser for chromosome 4 in K562 with an example of ADV aRTIL (in red). **b** Heatmap and clustering trees based on Pearson correlations for epigenetic marks coverage in K562 regions (ClusVis Software, ENCODE ChiP-seq data). **c** Boxplots of RT domains size (in kb) for Early, Mid, Late, ADV aRTIL and DEL aRTIL in K562 and RKO cell lines. **d** Boxplots of GC content in Early, Mid, Late, ADV aRTIL and DEL aRTIL genomic regions in K562 and RKO cell lines. **e** Boxplots of constitutive origins coverage in Early, Mid, Late, ADV aRTIL

and DEL aRTIL genomic regions in K562 and RKO cell lines. **f** Boxplots of gene coverage in Early, Mid, Late, ADV aRTIL and DEL aRTIL genomic regions in K562 and HCT116 cell lines. Statistics (for all the boxplots): Wilcoxon rank sum test ***p<0.005, *p<0.05, ns when p>0.05.

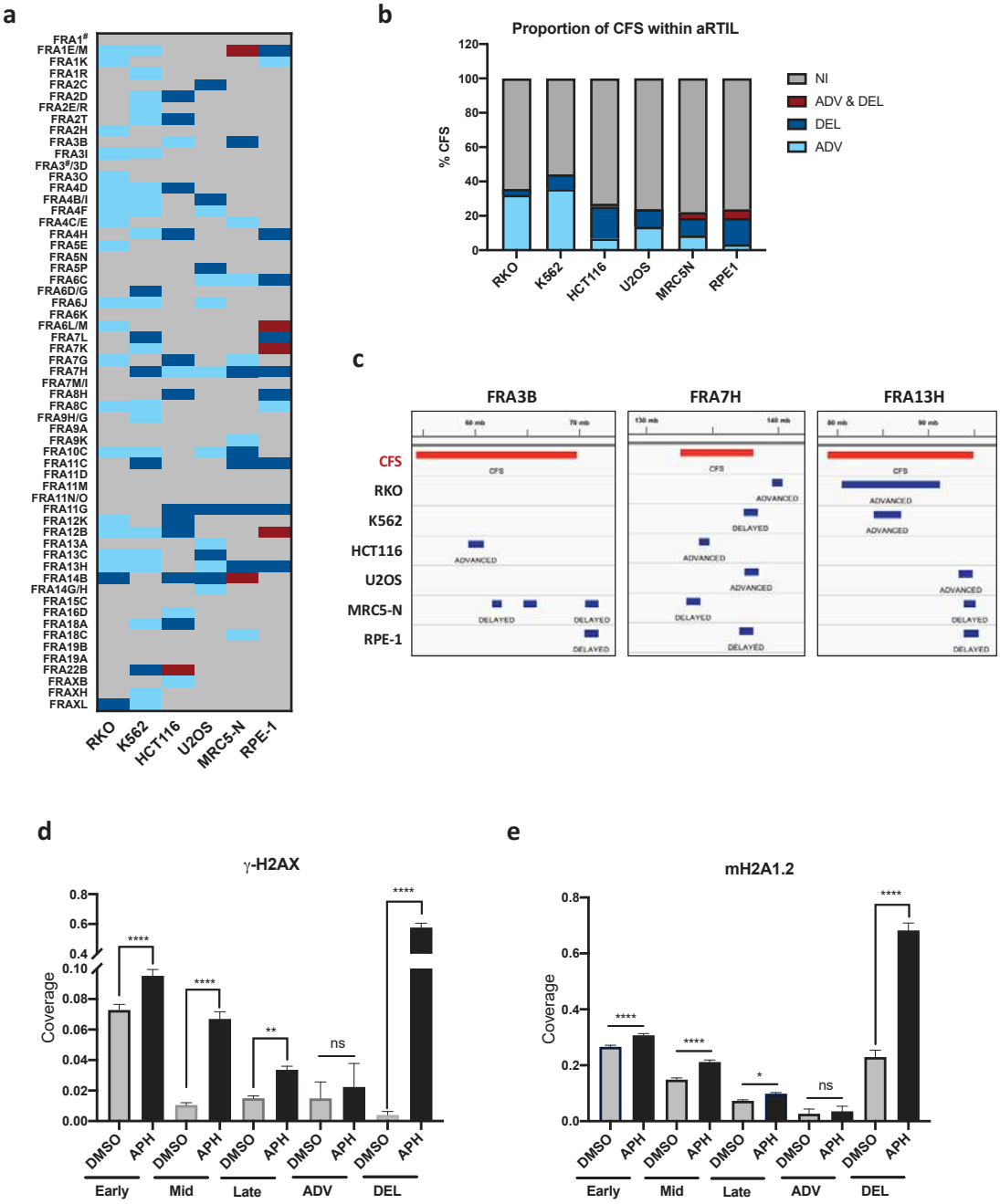

Figure 3: ADV aRTIL are closely related to CFSs but are not targeted by DNA damage signalling. a Categorical heatmap to visualize impacted CFS by aRTIL in all cell lines: ADV & DEL in dark red, DEL in dark blue, ADV in light blue and non-impacted (NI) in grey. **b** Histogram representing the proportion (in %) of CFSs within aRTIL. ADV & DEL in dark red, DEL in dark blue, ADV in light blue and non-impacted (NI) in grey. **c** Genome Browser (IGV) snapshots to visualize aRTIL (in blue) in all cell lines for three CFS (in red): FRA3B, FRA7H and FR13H. **d** Histogram representing the coverage of gH2AX histone mark (ChiP-seq data) on Early, Mid, Late, ADV aRTIL and DEL aRTIL genomic regions in DMSO and APH treated conditions. Statistics: Two-way ANOVA, Multiple comparison: ****p<0.0001, **p<0.01, *p<0.05, ns

p>0.05. **e** Histogram representing the coverage of mH2A1.2 histone mark (ChiP-seq data) on Early, Mid, Late, ADV and DEL aRTIL genomic regions in DMSO and APH treated conditions. Statistics: Two-way ANOVA, Multiple comparison: ****p<0.0001, **p<0.01, *p<0.05, ns p>0.05.

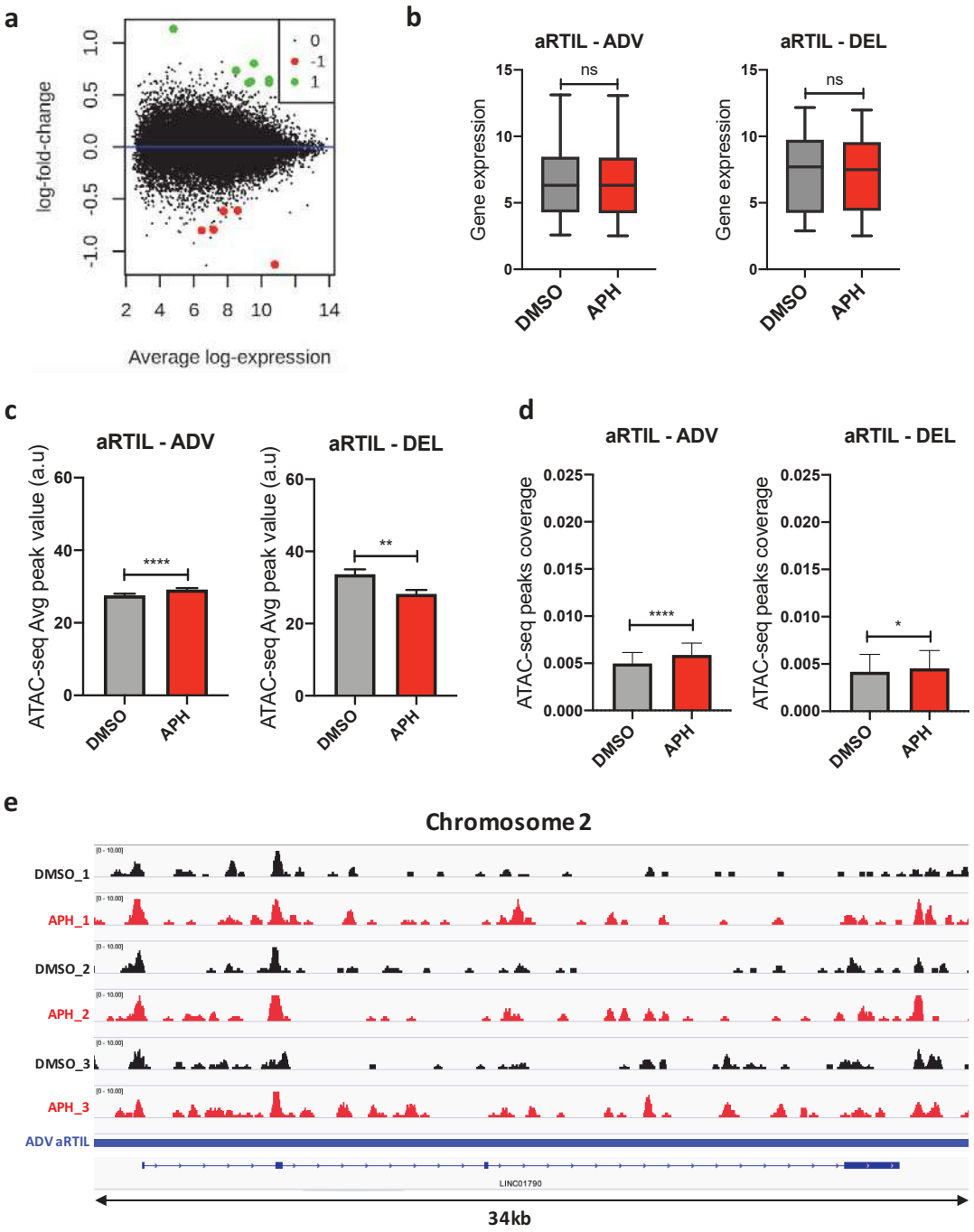

Figure 4: Aphidicolin modulates chromatin accessibility within ADV aRTIL without impacting gene expression. a Scatterplot for RNA-ChiP data in RKO cells representing significantly UP (green) and DOWN (red) -regulated genes in response to aphidicolin. **b** Boxplots measuring the expression of genes within ADV (left) and DEL (right) aRTIL in DMSO (grey) and APH (red) conditions. Statistics: Wilcoxon matched-pairs signed rank test ns p>0.05. **c** Comparison of ATAC-seq peak value within ADV and DEL aRTIL regions between DMSO (grey) and APH (red) conditions. **d** Comparison of ATAC-seq peak coverage within ADV and DEL aRTIL between DMSO (grey) and APH (red) conditions. Statistics (N=3): Wilcoxon matched-pairs signed rank

test ****p<0.0001, **p<0.01, *p<0.05. **e** Screenshot of integrative genome viewer (IGV) session with ATAC-seq triplicates bigwig files on chromosome 2 within a specific ADV aRTIL (194,728,595-194,763,435kb, LINC01790).

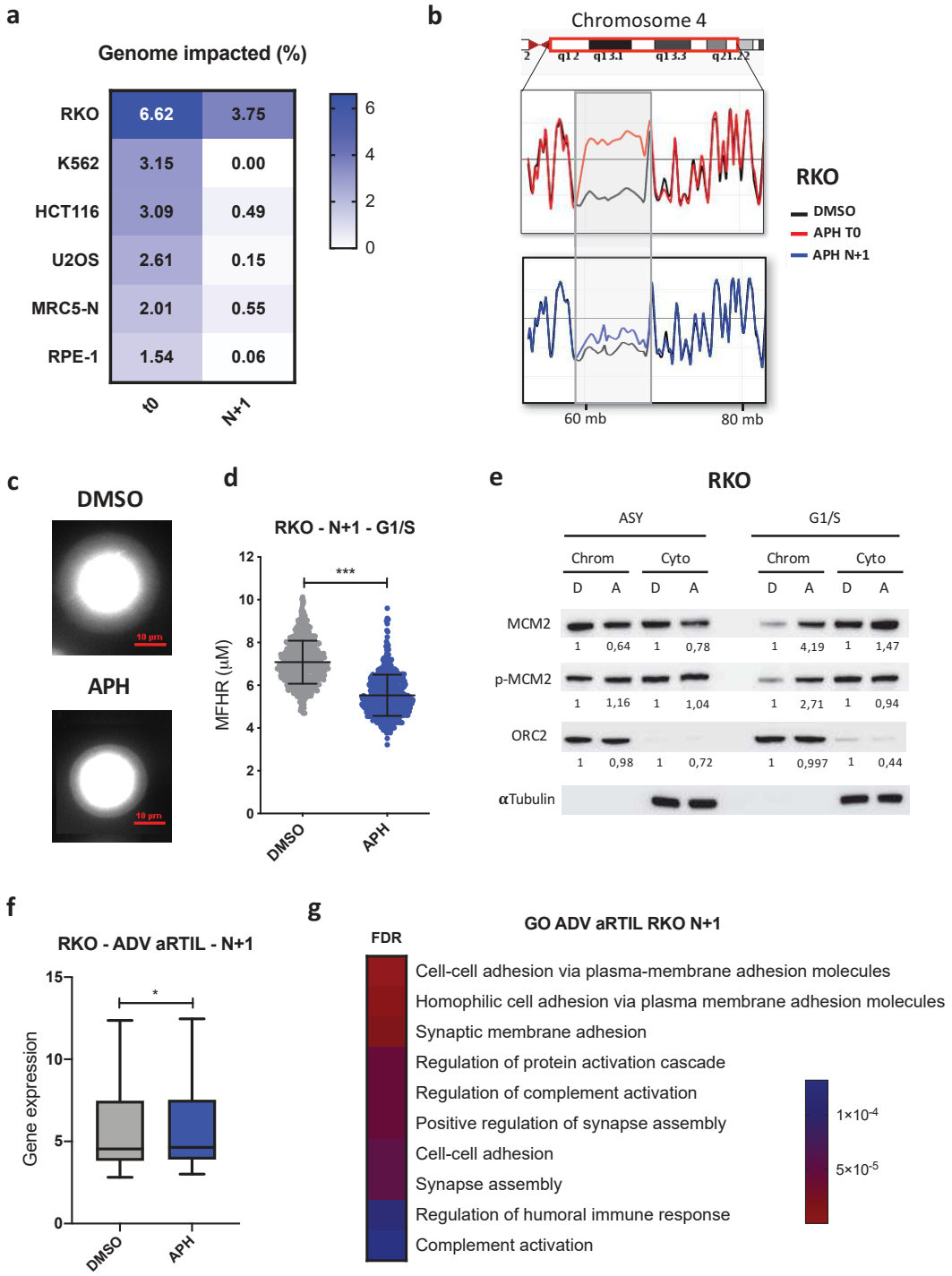

Figure 5: **ADV aRTIL can be transmitted to daughter cells. a** Heatmap representing the coverage (in %) of impacted genomic regions in mother cells (t0) or released daughter cells (N+1) for the six cell lines. **b** Screenshots of Loess-smooth replication timing profiles for the same region in chromosome 4 for RKO, in mother (APH T0) and daughter cells (APH N+1). The dark lines correspond to replication timing of control (DMSO) replication timing, the red line is replication timing of T0 APH treated cells and the blue line is the replication timing of N+1 daughter cells released from APH treatment. **c** Visualization and **d** Quantification of DNA Halo

size (MFHR) in RKO G1/S synchronized daughter cells released from DMSO or aphidicolin treatment. Statistics (N=3): Unpaired t test with Welch's correction ***p<0.001. **e** Western blot on chromatin (Chrom) and cytoplasmic (Cyto) protein fractions to quantify the amount of MCM2, p-MCM2 and ORC2 in asynchronous cells (ASY) and cells synchronized in G1/S with L-mimosine. The fold change between DMSO and APH condition measured in three independent experiments is reported on the figure. **f** Boxplot measuring the expression of genes within ADV aRTIL in DMSO and APH released daughter cells (N+1). Statistics: Wilcoxon matched-pairs signed rank test *p<0.05. **g** Gene ontology for RKO N+1 ADV aRTIL UP-regulated genes (ShinyGO, P-val cutoff: FDR < 0.05).